Relative detection sensitivity in ultrafast spectroscopy: state lifetime and laser pulse duration effects

Relative detection sensitivity in ultrafast spectroscopy: State lifetime and laser pulse duration effects

Nikoleta Kotsina[1] and Dave Townsend[1,2,*]

[1] *Institute of Photonics & Quantum Sciences, Heriot-Watt University, Edinburgh, EH14 4AS, United Kingdom*

[2] *Institute of Chemical Sciences, Heriot-Watt University, Edinburgh, EH14 4AS, United Kingdom*

Abstract

We present a numerical modelling study employing a kinetic model based on rate equations to investigate the role of excited state lifetime and laser pulse duration on effective relative detection efficiency in time-resolved pump-probe spectroscopy. The work begins to address the critical outstanding problem of photochemical branching ratio determination when excited state population evolves via competing relaxation pathways in molecular systems. Our findings reveal significant differences in detection sensitivity, which can exceed an order of magnitude under typical experimental conditions for excited state lifetimes ranging between 10 fs and 1 ps. We frame our discussion within the widely used approach of ultrafast photoionization for interrogating excited state populations, but our overall treatment may be readily extended to consider a broader range of experimental methodologies and timescales.

[*] Corresponding author. E-mail: D.Townsend@hw.ac.uk

I. INTRODUCTION

In recent years, photoionization-based methods for investigating time-resolved evolution of excited state populations following ultraviolet light absorption have become widely used to interrogate non-adiabatic molecular dynamics.[1-5] Non-adiabatic processes play a central role in many fundamentally important systems in biology (e.g. vison, light harvesting, photo-protection), atmospheric and interstellar photochemistry, and also in synthetic photostabilizers, photochromic polymers, sunscreens, molecular switches and drugs for the targeted delivery of active agents (photodynamic therapy).[5-14] Developing a more detailed understanding of non-adiabatic phenomena in molecules – and in particular the complex interplay between structure, dynamics and chemical function is therefore a hugely important challenge.

In time-resolved spectroscopic studies, the principal goal is to directly track population from a set of initially (optically) prepared electronic states – the photoreactants – towards a final set of photoproducts along the connecting nuclear reaction coordinates. This often involves multiple competing pathways that may operate in parallel and/or sequentially, passing (non-radiatively) through various intermediate electronic states on timescales ranging from a few femtoseconds to nanoseconds and beyond. Several variants of ionization-based detection are commonly employed to observe this dynamical evolution, including time-resolved ion-yield (TRIY), time-resolved photoelectron spectroscopy (TRPES) and time-resolved photoelectron imaging (TRPEI). These approaches have proved highly instructive in revealing subtle mechanistic details of critical relaxation pathways operating in a wide range of molecular systems. This is particularly true of the highly differential energy- and angle-resolved TRPEI technique, as illustrated, for example, by some of our own recent work[15-18] as well as that of others.[19-24]

One major limitation inherent to the experimental approaches mentioned above is that significant differences may exist in the relative effective sensitivity to ionization detection exhibited by various states participating in the overall relaxation process. This therefore means it is often problematic to characterise the relative importance of one decay pathway over another (i.e. the branching ratio) in a manner that is qualitative, let alone quantitative. This is an extremely challenging issue as numerous factors may contribute simultaneously to changes in effective ionization detection sensitivity along a given reaction coordinate and also between different competing reaction coordinates. These include the role of any excited state alignment effects, differences in relative electronic ionization cross-sections and vibrational Franck-Condon factors, coherent phenomena and differences in relative excited state lifetimes. Moreover, these various effects may not only manifest upon transferring population non-adiabatically between different electronic states (*inter*-state detection) but can also arise due to nuclear geometry changes within a given electronic state (*intra*-state detection). Furthermore, this situation may be additionally convoluted by any differences in relative absorption cross-sections when multiple states are prepared simultaneously during the initial excitation.

In some cases, a few of the effects outlined above may be overcome in a relatively straightforward manner. By making use of "magic-angle" pump-probe schemes, for example, excited state alignment effects may potentially be eliminated,[25] although this breaking of cylindrical symmetry is not always well-suited for use with the TRPEI approach. Alternatively, alignment effects may sometimes be robustly quantified using well-established angular momentum theory[26] or interrogated directly using techniques such as Coulomb explosion imaging.[27] Coherent phenomena (for example, periodic "quantum beats" superimposed on exponentially decaying pump-probe signals) may be de-convoluted from the overall state lifetime,[28, 29] and reliable absorption cross-sections are often also available from existing spectroscopic data. For other effects, however, the situation is more problematic. In particular,

the evaluation of photoionization cross-sections and Franck-Condon factors is presently extremely challenging and (from a theoretical standpoint) computationally intensive for the excited states of most polyatomic molecules. This is further compounded by the fact that such effects are dependent upon molecular geometry and therefore exhibit a time-dependence to which experimental measurements are sensitive. As a potential route to facilitating better qualitative discussion of these issues, we have previously argued it is appealing to seek correlations between, for example, electronic photoionization cross-sections and physical molecular properties that may be evaluated in a relatively straightforward and computationally inexpensive manner. A more detailed discussion is beyond the scope of this present study, but the reader is directed to our earlier work that begins exploring correlations between isotropic polarizability volume and electronic photoionization cross-section for some initial, albeit speculative thoughts on this issue.[18, 30]

In this communication, we present a generalized numerical modelling study that quantifies effective sensitivity to ionization detection of excited states as a function of their lifetime relative to the temporal duration of exciting/ionizing laser pulses. We aim to isolate the dependence of the recorded signal as a function of the laser pulse characteristics, free from any molecule-specific properties. A full quantum mechanical treatment simulating the preparation of the molecular system under the influence of pump and probe pulses is beyond the scope of this work, although we highlight that several articles have previously addressed this issue in some way.[31-39] For simplicity, however, quantum mechanical descriptions often treat the excitation/ionization processes as instantaneous, i.e. the pulses are represented by delta functions and, as a result, any influence on detected signal levels due to the pulse duration is ignored.[39] Moreover, quantum calculations often also consider the limit of non-temporally overlapping pump-probe pulses in an attempt to further simplify the problem.[33, 34, 39] As an alternative strategy, a simple treatment based on kinetic modelling and rate equations is well-

suited for mapping the influence of laser pulse characteristics and state lifetime effects in a practically useful and broadly applicable manner.[40, 41] Although, as already highlighted, these two parameters are just a small subset of the many factors contributing to overall relative ionization detection efficiency, their role is reasonably straightforward to evaluate. Moreover, the potentially significant variation in the size of the influence they exert (discussed below) means our findings represent an important step in moving towards more quantitative discussions of branching ratios in many ultrafast molecular dynamics experiments. One important aim of this communication is therefore to provide clearly presented information to aid heuristic interpretation of TRIY, TRPES and TRPEI data for realistic sets of experimental parameters. More broadly, our work also aims to highlight the need to undertake additional, much wider-reaching investigations addressing the overall issue of relative ionization detection sensitivity – especially since the use of the TRIY, TRPES and TRPEI techniques has become so widespread in the study of non-adiabatic photochemical dynamics.

II. DIRECT OPTICAL PREPARATION WITH SINGLE-PHOTON DETECTION

We begin by considering the detection sensitivity problem when population transfer into an excited state is achieved via direct interaction with a pump laser pulse. Our treatment omits the potential role of saturation effects, which is reasonable for the low-flux ($< 10^{11}$ W/cm^2), single-photon absorption typically used in the types of experiments being addressed. The electric field envelope of the laser pulse is taken as Gaussian, with a half width at 1/*e* of the peak maximum denoted by σ (although the discussion outlined below can easily be modified to other pulse profiles, i.e Lorentzian, hyperbolic secant etc.). We then formulate our treatment in terms of intensity (the square of the electric field) as this is typically the measured quantity in real experiments – as estimated by considering various laser beam parameters and the degree of focusing at the point of interaction with a molecular sample. In terms of pulse normalization there are two basic approaches; either to consider constant peak

power (where the maximum amplitude of the pulse is fixed as the width is varied) or constant average power (where the area under the pulse remains invariant and is set to unity). Since both cases are of interest when comparing different experimental data sets, we consider both situations here. The Gaussian pulse is described by the following equation;

$$g(t) = Ne^{-2(t/\sigma)^2} \tag{1}$$

Here $N = 1$ or $1/(\sqrt{\pi/2}\sigma)$ for the constant peak power and constant average power cases, respectively. Under such conditions the interaction is as follows:

$$f_p(\sigma,\tau,t) = \int_{-\infty}^{+\infty} \Theta(t-t')g(t')e^{-(t-t')/\tau}dt' \tag{2}$$

Here $\Theta(t-t')$ is the unit-step function and τ is the lifetime of the (exponentially decaying) excited state. The use of an exponential function to approximate the lifetime assumes a statistical limit where the density of non-adiabatically coupled (vibrational) states is sufficiently large to provide an apparent quasi-continuum.[42] Such a situation is extremely common in the excited states of polyatomic molecules, as evidenced by the near-ubiquitous use of exponential fitting to model time-resolved spectroscopic data. The quantity f_p describes evolution of population in the excited state and the system evolves as per Eq. 2, up to the moment when a second, probe laser pulse induces single-photon ionization. For the purposes of simplifying the discussion, the probe pulse is identical to the pump. The probe interaction is therefore:

$$S(\sigma,\tau,\Delta t) = \int_{-\infty}^{+\infty} g(t-\Delta t).f_p(\sigma,\tau,\Delta t)\,dt \tag{3}$$

Here Δt denotes the time difference between the maxima of the pump and probe pulses and S is the resultant ionization signal (the actual observable in a real experiment), which depends on the properties of the pump/probe laser pulses (σ, Δt) and the excited state lifetime (τ). Eq. 3 assumes all population within the excited state is ionized with equal probability, i.e. any

molecule-specific properties such as Franck-Condon factors are not included as such effects may be considered separately. The aim here is to isolate and parametrise only the lifetime and pulse duration effects. After substituting for $f_p(\sigma,\tau,\Delta t)$, when $\sigma > 0$ and $\tau > 0$, Eq. 3 then becomes:

$$S(\sigma,\tau,\Delta t) = \alpha e^{(\sigma/(2\sqrt{2}\tau))^2} \int_{-\infty}^{+\infty} e^{-2((t-\Delta t)/\sigma)^2} e^{-t/\tau} erfc\left[\frac{\sigma}{2\sqrt{2}\tau} - \frac{\sqrt{2}t}{\sigma}\right] dt \qquad (4)$$

Here $\alpha = \sigma\sqrt{\pi/8}$ or $1/(\sqrt{2\pi}\sigma)$ for the constant peak power and constant average power case, respectively, and *erfc* is the complementary error function. The influence of the parameters σ, Δt and τ on *S* may now be investigated using Eq. 4 and this was undertaken numerically using Mathematica 11.0.[43] In all findings presented subsequently, σ values are recast in terms of the corresponding full-width at half-maximum (FWHM) values since this is a more commonly reported measure of laser pulse duration (and overall instrument response function) in time-resolved experiments. For Gaussian pulses the two quantities are connected via FWHM = $\sqrt{2\ln 2}\sigma$. For ease of comparison across all plots shown, the data are scaled relative to the value obtained for *S* with input parameters of FWHM = 100 fs, τ = 100 fs and Δt = 0.

Initially, a wide range of excited state lifetimes and laser pulse widths were considered for the situation where the pump and probe pulses are perfectly overlapped in time (i.e. Δt = 0). This data is presented in Fig. 1(a) for constant peak power and reveals significant differences in relative ionization signals for lifetimes between 10 fs and 1 ps. This is an immediately important outcome. For example, consider a situation where two different (fully uncoupled) electronic states exhibit identical absorption and ionization cross-sections but differ in their exponential decay lifetime, with one being 50 fs and the other 1 ps. Now consider simultaneous excitation and subsequent ionization of these states in a pump-probe experiment using 100 fs FWHM laser pulses - a duration typically representative of that presently employed in many

ultrafast spectroscopic measurements. The data in Fig. 1(a) predict this situation would yield photoelectron (or photoion) signals (at $\Delta t = 0$) from the 1 ps lifetime state that are a factor of 2.0 larger than for the 50 fs lifetime state. Clearly this simple illustration immediately highlights lifetime and laser pulse duration effects as a significant consideration in making even qualitative arguments about the relative importance of one state over another in contributing to the overall system decay process. It is interesting here to now compare Fig. 1(a) to Fig. 1(b) where we have again considered the condition $\Delta t = 0$, but for constant average power. At first glance the two figures look somewhat different, but a closer inspection reveals both give the same information on relative detection sensitivity for a given FWHM value. For example, if we again consider the case of two states with lifetimes of 50 fs and 1 ps being simultaneously excited by a 100 fs pulse, Fig. 1(b) also predicts that the signal from the 1 ps state will be the same factor of exactly 2.0 larger than from the 50 fs state. The difference in the appearance of the two figures is simply related to the peak/average power definition (which only scales the relative signal levels differently as the pulse FWHM is varied) rather than any lifetime dependence. The observed differences also make sense in the limiting case where the pulse FWHM tends to zero. From the constant average power perspective this means that the pulse is given by a delta function with a peak amplitude that tends to infinity, giving rise to a signal reflecting the molecular response function free from the influence of any pulse duration effects.[41] From the perspective of constant peak power, however, the relative signal size tends to zero as the peak amplitude remains the same as temporally broader pulses which deliver far greater total energy to the sample under study.

We may now also consider transient ionization signals obtained for various laser pulse widths (i.e. when Δt is varied, as in a time-resolved experimental measurement). This is illustrated in Fig. 2(a) – (f) for both constant peak power and constant average power conditions when τ = 10 fs, 100 fs and 1 ps. For a given state lifetime, it is clear that when the peak power

is kept constant (a) – (c) there is a marked increase in detection sensitivity as pulse duration increases. For constant average power (d) – (f), however, the signal decreases for longer pulse durations. This latter case is well-known from an experimental point of view, for example, when adjusting laser pulse chirp any observed signal will drop as the pulses deviate from optimal compression. Far more instructively, transient ionization signals obtained for selected laser pulse durations of 25 fs, 100 fs and 200 fs FWHM are shown for the case of constant peak power in Fig. 3(a) – (c). For a given pulse duration, the overall appearance of the 3-D plots is identical for the constant average power regime, reflecting the fact that the choice of normalization of the Gaussian pulse plays no critical role here – i.e. σ is a fixed quantity in each individual plot and the choice of pulse normalization scheme simply changes the scaling of the intensity axes. The data presented in Fig. 3(a) – (c) represent a key central result of our present work. This is the situation relating directly to the issue of relative excited state detection sensitivity (and therefore branching ratio determination) within a given experimental pump-probe measurement – i.e. where the laser pulse FWHM is constant, but various states with different lifetimes may be prepared simultaneously. In all instances, relative ionization efficiency increases with excited state lifetime, but the absolute magnitude of this change varies dramatically with pulse duration: For the 25 fs FWHM example relative detection sensitivity increases by a factor of ~3 over the range between τ = 100 fs and 1 ps, whereas this effect is much larger (a factor of ~8) over the same range when 200 fs FWHM laser pulses are employed.

In order to present data such as that shown in Fig. 3 in a more convenient form for use in a practical context, Fig. 4 presents the *maximum* relative photoionization efficiency obtained for a range of excited state lifetimes at selected laser pulse widths. As is evident from Fig. 3, this maximum occurs at pump-probe delays that are displaced increasingly away from zero as the excited state lifetime extends. Relative differences in the signal maximum may then be used

to rescale transient amplitude analysis conducted on experimental data using multiple exponential fitting functions, factoring out the influence of laser pulse duration and state lifetime effects.

For a salient practical example of where the data in Fig. 4 may might be instructively applied, we now draw on our recent TRPEI work on methyl-substituted aniline derivatives.[44] A detailed discussion of the findings is beyond the scope of this communication, but we highlight that, on the basis of what might reasonably be predicted from absorption cross section data alone, there appear to be significant discrepancies in the relative photoelectron signal levels observed following ionization of specific excited states. This is particularly true for the long-lived (> 100 ps) $S_1(\pi\pi^*)$ and very short-lived (< 10 fs) $2\pi\pi^*$ excited states of these systems. We believe this may, at least in part, be rationalized by invoking effective detection sensitivity *vs* lifetime and laser pulse duration effects. To demonstrate this point, Fig. 5 (a) presents a series of decay associated spectra (DAS) obtained for *N*,*N*-dimethylaniline following 240 nm excitation. The DAS are a plot of relative amplitude *vs* photoelectron kinetic energy for each individual exponential fitting function applied to an experimental data set (i.e. a photoelectron spectrum evolving in time as a function of pump-probe delay). In this specific example, four exponentially decaying functions that all originate from zero pump-probe delay were used, with associated time constants spanning a broad range between <10 fs (taken to be effectively Gaussian in the original publication[44]) and 150 ps. The instrument response function (i.e. pump-probe cross-correlation) was 130 fs FWHM and so we assume that the individual (de-convoluted) pump and probe pulses are both ~150 fs FWHM.

Making use of the information given above and the data in Fig. 4, Fig 5 (b) now presents the DAS following rescaling for lifetime and laser pulse duration effects. It is immediately apparent that the spectrum associated with the very short time constant τ_1 < 10 fs increases enormously in overall relative amplitude. The gain here is approximately a factor of 25 relative

to the DAS with time constant τ_4 = 150 ps. Furthermore, although the relative amplitude of the DAS for which τ_2 = 120 fs falls in relative amplitude *vs* the τ_1 DAS, is also gains in amplitude (by a factor of approximately 2) relative to the long-lived τ_4 DAS. The rescaling here effectively corrects for the "under-sampling" of population passing through very short-lived excited states and, critically, is demonstrated in this example to be a very significant effect.

III. THE ROLE OF MULTI-PHOTON IONIZATION

Eq. (4) is applicable only to (1+1) or (1+1′) resonant ionization schemes, i.e. when one photon from the pump pulse transfers population from the electronic ground state to an excited state and one photon from the probe pulse then induces photoionization. To also investigate multiphoton ionization processes in our model, Eq. (3) may be modified as follows:

$$S(\sigma,\tau,\Delta t,n) = N\int_{-\infty}^{+\infty} e^{-2n((t-\Delta t)/\sigma)^2}.f_p(\sigma,\tau,\Delta t)\,dt \qquad (5)$$

Here, as previously, N = 1 or $1/(\sqrt{\pi/2}\sigma)$ for the constant peak power and constant average power cases, respectively. Additionally, n is the photon order of the probe pulse – i.e. we are now considering (1+n) or (1+n') ionization schemes, as are often employed in many time-resolved pump-probe measurements. As a simplifying assumption, we do not consider the possibility of the system being excited through any additional resonances (which would introduce additional lifetime effects) during the multiphoton ionization step. To investigate the photon order effect, the full 3D plots presented in Fig. 1 were recalculated for several specific individual n values. The overall shape and general trend behaviour of these plots remain qualitatively very similar to the single photon ionization case considered previously, and are therefore not shown here. This is an expected result since, as is evident from Eq. 4, increasing the photon order effectively results in a temporally shorter interaction between the system and the probe pulse, but which is still described by a Gaussian form. What is more relevant here is to plot the ionization signal S as a function of n and τ. To quantify any dependence, Fig. 6

shows the variation in ionization efficiency $S(\text{FWHM} = 100\ \text{fs}, \tau, \Delta t = 0, n)$ for selected lifetimes spanning τ = 50 fs - 10 ps over multiphoton ionization orders n = 1-8. Data points for each specific photon order are scaled relative to FWHM = 100 fs, Δt = 0, τ = 100 fs in each case as the relative change in detection sensitivity as a function of lifetime for a given n is of most relevance for practical experimental considerations (i.e. a given experiment with fixed pulse FWHM where multiple states with different lifetimes are prepared simultaneously and ionized via the same (1+n') process). This scaling also means that there is no difference between the constant peak power and constant average perspectives, and both approaches produce the same output. At all selected τ values, S exhibits only a weak dependence on n. For lifetimes longer/shorter than 100 fs, S falls/rises slightly as the photon order initially increases, converging towards a fixed value in the high n limit. Overall, the influence of the ionization photon order on effective relative detection is far less significant than the other parameters already investigated (see Fig. 1). We will therefore not consider multiphoton ionization processes any further in the remainder of this communication and limit subsequent discussions to resonant (1+1) or (1+1′) schemes.

IV. SEQUENTIAL PROCSSES

The data presented up to now are instructive when considering *parallel* dynamical processes in a given experimental measurement (i.e. multiple excited states are simultaneously prepared in the pump step and undergo fully independent decay). We now, however, seek to extend our treatment and consider a scheme applicable to *sequential* dynamical processes, i.e. those where an “optically dark” excited state (hereafter referred to as State B) is prepared via a non-radiative process from a different “optically bright” state (State A) that undergoes loss of population via exponential decay. Note that “optically bright and “optically dark” here refer to the *absorption* properties of the two states – i.e. the initial step in the overall (1+1) or (1+1′) process – and not their ionization properties, which we assume to be identical for the simplified

treatment we are presenting. As with the parallel processes considered earlier, we are isolating and parametrising just the influence of the excited state lifetime and laser pulse duration on overall relative detection sensitivity. In this situation, the evolution of State B population is now as follows:

$$f_s(\sigma,\tau_1,\tau_2,t) = \int_{-\infty}^{+\infty} \Theta(t-t') \left(\int_{-\infty}^{+\infty} \Theta(t'-t'') \frac{g(t'')}{\tau_1} e^{-(t'-t'')/\tau_1} dt'' \right) e^{-(t-t')/\tau_2} dt' \quad (6)$$

This expression is similar to Eq. 2, but now the (Gaussian) optical pump term is replaced with a function describing an exponential growth of State B population with a time constant τ_1 (that also describes simultaneous loss of population from State A). This new function also has a dependence on the temporal width of the optical pump pulse used to prepare State A initially. The subsequent exponential decay of population from State B is then described by a second time constant τ_2. The observed ionization signal S is now obtained by replacing f_p with f_s in Eq. (3), noting also that the factor α is defined in the same way as for Eq. 4:

$$S(\sigma,\tau_1,\tau_2,\Delta t) = \alpha \frac{\tau_2}{(\tau_1-\tau_2)} \times \int_{-\infty}^{+\infty} \left\{ \begin{array}{l} e^{-2((t-\Delta t)/\sigma)^2} [e^{(\sigma/(2\sqrt{2}\tau_1))^2 - t/\tau_1} (1 + erf\left[\frac{\sqrt{2}t}{\sigma} - \frac{\sigma}{2\sqrt{2}\tau_1} \right]) \\ \qquad + e^{(\sigma/(2\sqrt{2}\tau_2))^2 - t/\tau_2} (-2 + erfc\left[\frac{\sqrt{2}t}{\sigma} - \frac{\sigma}{2\sqrt{2}\tau_2} \right])] \end{array} \right\} dt \quad (7)$$

We may now investigate variation in S with respect to σ, τ_1, τ_2 and Δt. Since this is a four-dimensional parameter space, we simplify presentation of our analysis by restricting the following discussion to selected State A lifetimes of τ_1 = 100 fs, 500 fs and 1 ps, in combination with 100 fs FWHM Gaussian pump and probe pulses. Keeping the FWHM constant also means that there will be no difference between the constant peak power and constant average power cases (as already illustrated in Fig. 1). For our choices of initial conditions, Fig. 7 presents variation in S as a function of Δt for a range of selected State B decay lifetimes τ_2. Specifically,

in Fig. 7(a) the initially populated State A exhibits a relatively short lifetime $\tau_1 = 100$ fs, meaning that any population decays extremely rapidly into State B and, consequently, its ionization signal will be rather weak. The corresponding ionization signal from State B is similarly weak when $\tau_2 = 200$ fs but doubles in size once $\tau_2 = 5$ ps. In Fig. 7(b) the State A τ_1 lifetime is now 500 fs. In this case the relative ionization signal from State B is significantly weaker when $\tau_2 < 1$ ps, and only becomes comparable to the State A intensity once τ_2 is ~5 ps (a value ten times that of τ_1). This general trend is also apparent in Fig. 7(c) where the State A lifetime is set to $\tau_1 = 1$ ps. Here the relative size of the ionization signal originating from State B is now always weaker over the full range of τ_2 values sampled. Finally, we consider an interesting set of outcomes that are summarized in Fig. 7(d). As with Fig. 7(c), the State A lifetime $\tau_1 = 1$ ps but now the State B lifetimes τ_2 have been selected over the range 50-800 fs (i.e. now $\tau_1 > \tau_2$). The ionization signal from State B is now always considerably weaker than that from State A (in some cases an order of magnitude smaller). This is simply a consequence of population not accumulating significantly in the short-lived State B, which is now (especially for the $\tau_2 = 50$ fs case) starting to exhibit the well-known "steady state" behaviour that is a familiar concept in elementary chemical kinetics. Fig. 7(d) therefore also demonstrates that information on the State B lifetime is now revealed differently in the observed ionization signal. In Fig. 7(a)-(c), where $\tau_2 > \tau_1$, any information relevant to the lifetime of the State B can be extracted by simply fitting an exponentially decaying function to the raw data, while the precursor lifetime τ_1 appears as the exponential rise. When $\tau_1 > \tau_2$, however, this is no longer the case. State B now gives rise to a weak, pseudo long-lived ionization signature that does not directly reflect the actual lifetime and, in the limit where $\tau_1 >> \tau_2$, the τ_2 lifetime effectively follows that of τ_1. This pseudo lifetime effect is potentially an important consideration when conducting and interpreting any time-dependent analysis of experimental data obtained using

techniques such as TRIY, TRPES and TRPEI. The actual state lifetime τ_2 appears now instead as the exponential rise.[41]

V. CONCLUSION

In summary, we have presented numerical modelling studies investigating the influence of excited state lifetime and laser pulse duration on effective relative detection efficiency in photoionization-based pump-probe molecular spectroscopy. We employ a simple kinetic treatment from the perspective of both constant peak power and constant average power, although for the key results (detection of different excited states in a single experiment with a fixed lase pulse width) the two regimes predict identical behaviour. Although addressing only a small subset of overall contributing factors, the work makes straightforward and broadly applicable first steps towards addressing an often-ignored limitation of time-resolved measurements – namely the reliable determination of branching ratios when tracking non-adiabatic evolution of excited state population via competing relaxation pathways. Significantly, for laser pulse widths commonly used in many ultrafast pump-probe experiments, our findings reveal differences in detection sensitivity can exceed an order of magnitude for state lifetimes varying between 10 fs and 1 ps. Quantifying the size of these effects is therefore clearly of importance in moving towards more robust discussions of photoproduct branching when employing techniques such as TRIY, TRPES and TRPEI to interrogate non-adiabatic dynamics in the excited states of molecules. Our findings consider both simple parallel and sequential decay mechanisms and may therefore be readily extended to more complex experimental data involving multiple, multi-step relaxation pathways. This includes the possibility of rescaling transient amplitude analysis (once excited state lifetimes have been determined) to factor out the laser pulse duration effects – as we have illustrated using some of our own experimental TRPEI data. This would also allow independent pump-probe measurements conducted on the same molecular system but with different temporal

resolution to be compared more directly. Furthermore, our work also highlights important caveats in the assignment of temporal features arising from sequential dynamical processes where $\tau_1 > \tau_2$. Given the extremely widespread use of the TRIY, TRPES and TRPEI techniques, we anticipate our overall findings will be of broad interest to the time-resolved spectroscopy and dynamics community and significantly influence future work in this area. Furthermore, the general ideas outlined here in regard to relative detection sensitivity are also applicable to wider range of time-resolved experimental methodologies and timescales, and we highlight that our overall treatment may be readily adapted to such situations.

ACKNOWLEDGEMENTS

This study was made possible by financial support from Engineering and Physical Sciences Research Council (EPSRC) grants EP/P001459/1 and EP/K021052/1. Associated data are deposited with the Heriot-Watt Research Archive.

REFERENCES

1. A. H. Zewail, *J. Phys. Chem. A*, 2000, **104**, 5660.
2. A. Stolow, A. E. Bragg and D. M. Neumark, *Chem. Rev.*, 2004, 1719.
3. A. Stolow and J. G. Underwood, in *Advances in Chemical Physics*, ed. S. A. Rice, John Wiley & Sons, Inc., Hoboken, NJ, USA2008, vol. 139, pp. 497-583.
4. T. Suzuki, *Int. Rev. Phys. Chem.*, 2012, **31**, 265.
5. G. M. Roberts and V. G. Stavros, *Chem. Sci.*, 2014, **5**, 1698.
6. V. Sundström, *Annu. Rev. Phys. Chem.*, 2008, **59**, 53.
7. P. Kukura, D. W. McCamant, S. Yoon, D. B. Wandschneider and R. A. Mathies, *Science*, 2005, **310**, 1006.
8. C. E. Crespo-Hernández, B. Cohen, P. M. Hare and B. Kohler, *Chem. Res.*, 2004, **104**, 1977.
9. J. C. Tully, *J. Chem. Phys.*, 2012, **137**, 22A301.
10. S. Maeda, T. Taketsugu, K. Ohno and K. Morokuma, *J. Am. Chem. Soc.*, 2015, **137**, 3433.
11. G. Cui and W. Fang, *J. Chem. Phys.*, 2013, **138**, 044315.
12. M. Pollum and C. E. Crespo-Hernández, *J. Chem. Phys.*, 2014, **140**, 071101.
13. M. Pederzoli, J. Pittner, M. Barbatti and H. Lischka, *J. Phys. Chem. A*, 2011, **115**, 11136.
14. L. A. Baker, L. C. Grosvenor, M. N. R. Ashfold and V. G. Stavros, *Chem. Phys. Lett.*, 2016, **664**, 39.
15. J. O. F. Thompson, L. B. Klein, T. I. Sølling, M. J. Paterson and D. Townsend, *Chem. Sci.*, 2016, **7**, 1826.
16. L. B. Klein, J. O. F. Thompson, S. W. Crane, L. Saalbach, T. I. Sølling, M. J. Paterson and D. Townsend, *Phys. Chem. Chem. Phys.*, 2016, **18**, 25070.
17. L. B. Klein, T. J. Morsing, R. A. Livingstone, D. Townsend and T. I. Sølling, *Phys. Chem. Chem. Phys.*, 2016, **18**, 9715.
18. J. O. F. Thompson, L. Saalbach, S. W. Crane, M. J. Paterson and D. Townsend, *J. Chem. Phys.*, 2015, **142**, 114309.
19. V. Svoboda, N. B. Ram, R. Rajeev and H. J. Wörner, *J. Chem. Phys.*, 2017, **146**, 084301.
20. A. Röder, K. Issler, L. Poisson, A. Humeniuk, M. Wohlgemuth, M. Comte, F. Lepetit, I. Fischer, R. Mitric and J. Petersen, *J. Chem. Phys.*, 2017, **147**, 013902.
21. D. A. Horke, H. M. Watts, A. D. Smith, E. Jager, E. Springate, O. Alexander, C. Cacho, R. T. Chapman and R. S. Minns, *Phys. Rev. Lett.*, 2016, **117**, 163002.
22. T. Horio, Y.-I. Suzuki and T. Suzuki, *J. Chem. Phys.*, 2016, **145**, 044307.
23. Y. Liu, G. Knopp and T. Gerber, *Phys. Rev. A*, 2015, **92**, 042501.
24. J. N. Bull, C. W. West and J. R. R. Verlet, *Chem. Sci.*, 2015, **6**, 1578.
25. D. J. Leahy, K. L. Reid and R. N. Zare, *J. Chem. Phys.*, 1991, **95**, 1757.
26. R. N. Zare, *Angular Momentum: Understanding Spatial Aspects in Chemistry and Physics*, Wiley, New York, 1988.
27. Z. Vager, R. Naaman and E. P. Kanter, *Science*, 1989, **244**, 426.
28. A. E. Boguslavskiy, M. S. Schuurman, D. Townsend and A. Stolow, *Faraday Discuss.*, 2011, **150**, 419.
29. R. Spesyvtsev, T. Horio, Y.-I. Suzuki and T. Suzuki, *J. Chem. Phys.*, 2015, **142**, 074308.
30. M. M. Zawadzki, J. O. F. Thompson, E. A. Burgess, M. J. Paterson and D. Townsend, *Phys. Chem. Chem. Phys.*, 2015, **17**, 26659.

31. J. K. Freericks, H. R. Krishnamurthy and T. Pruschke, *Phys. Rev. Lett.*, 2009, **102**, 136401.
32. M. Joffre, in *Femtosecond Laser Pulses Principles and Experiments*, ed. C. Rullière, Springer, New York2004, p. 283.
33. N. E. Henriksen and V. Engel, *Int. Rev. Phys. Chem.*, 2001, **20**, 93.
34. K. B. Møller, N. E. Henriksen and A. H. Zewail, *J. Chem. Phys.*, 2000, **113**, 10477.
35. D. M. Jonas, S. E. Bradforth, S. A. Passino and G. R. Fleming, *J. Phys. Chem.*, 1995, **99**, 2594.
36. M. Braun, C. Meier and V. Engel, *J. Chem. Phys.*, 1995, **103**, 7907.
37. G. Stock and W. Domcke, *J. Opt. Soc. Am. B*, 1990, **7**, 1970.
38. L. E. Fried and S. Mukamel, *J. Chem. Phys.*, 1990, **93**, 3063.
39. Y. J. Yan, L. E. Fried and S. Mukamel, *J. Phys. Chem.*, 1989, **93**, 8149.
40. W. Fuß, W. E. Schmid and S. A. Trushin, *J. Chem. Phys.*, 2000, **112**, 8347.
41. S. Pedersen and A. H. Zewail, *Mol. Phys.*, 1996, **89**, 1455.
42. M. Bixon and J. Jortner, *J. Chem. Phys.*, 1968, **48**, 715.
43. Wolfram Research, Inc., Mathematica, Version 11.0, Champaign, IL (2016).
44. M. M. Zawadzki, M. Candelaresi, L. Saalbach, S. W. Crane, M. J. Paterson and D. Townsend, *Faraday Discuss.*, 2016, **194**, 185.

Figure Captions

Figure 1: Relative photoionization efficiency as a function of (Gaussian) FWHM laser pulse width and (1/*e*) excited state lifetime τ at zero pump-probe delay Δt = 0 under conditions of (a) constant peak power (CPP) or (b) constant average power (CAP). Pump and probe pulses are identical and the absorption/ionization cross-sections for the overall (1+1) process are assumed constant throughout. All intensities are scaled relative to that obtained at Δt = 0 for 100 fs FWHM pulses and τ = 100 fs.

Figure 2: Relative photoionization efficiency as a function of Δt and laser pulse FWHM for selected excited state lifetimes (τ = 10 fs, 100 fs and 1 ps) under conditions of constant peak power (CPP) (a) – (c) or constant average power (CAP) (d) – (f). Pump and probe pulses are identical and the absorption/ionization cross-sections for the overall (1+1) process are assumed constant throughout. All intensities are scaled relative to that obtained at Δt = 0 for 100 fs FWHM pulses and τ = 100 fs.

Figure 3: Relative photoionization efficiency as a function of Δt and τ for selected laser pulse widths (FWHM = 25 fs, 100 fs and 200 fs). Pump and probe pulses are identical and the absorption/ionization cross-sections for the overall (1+1) process are assumed constant throughout. All intensities are scaled relative to that obtained at Δt = 0 for 100 fs FWHM pulses and τ = 100 fs. Data is shown for the constant peak power regime – for more details see main text.

Figure 4: Maximum relative photoionization efficiency obtained for a range of excited state lifetimes at selected laser pulse widths: (a) FWHM = 200 fs, 150 fs and 100 fs, (b) FWHM = 100 fs, 50 fs and 25 fs. Pump and probe pulses are identical and the absorption/ionization cross-sections for the overall (1+1) process are assumed constant throughout. All intensities are scaled relative to that obtained at Δt = 0 for 100 fs FWHM pulses and τ = 100 fs.

Figure 5: (a) Decay associated spectra (DAS) obtained from a global multi-exponential fit to experimental TRPEI data obtained from *N*, *N*-dimethylaniline following 240 nm excitation. Comprehensive additional details may be found in Ref. 44. (b) The same data following re-scaling of the relative DAS amplitudes using the data presented in Fig. 4 and then subsequent re-normalization with respect to the most intense peak feature overall. See main text for further information.

Figure 6: Relative photoionization efficiency for five selected (1/*e*) exited state lifetimes (τ = 20 fs, 50 fs, 100 fs, 1 ps, and 10 ps) as a function of ionizing (i.e. probe) photon order *n* at zero pump-probe delay $\Delta t = 0$. All data points for a given photon order are scaled relative to the intensity value obtained at zero pump-probe delay for 100 fs FWHM pulses, exciting and then ionizing a state exhibiting a lifetime of 100 fs. The pump and *n* probe pulses are identical in all cases. For more details see the main text.

Figure 7: Relative photoionization efficiency as a function of pump-probe delay for an "optically dark" excited state (State B) with (1/*e*) lifetime τ_2 prepared via non-radiative population transfer from an "optically bright" excited state (State A) exhibiting τ_1 lifetimes of (a) 100 fs, (b) 500 fs, (c)-(d) 1 ps. For cases (a)-(c) $\tau_2 > \tau_1$, while for case (d) $\tau_1 > \tau_2$. Pump and probe pulses are identical and the absorption/ionization cross-sections for the overall (1+1) process are assumed constant throughout. All intensities are scaled as per the data in Fig. 3.

Fig 1

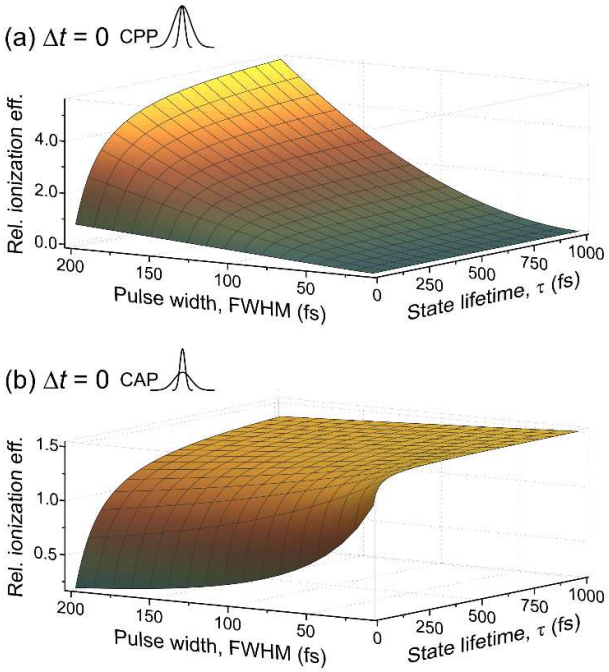
(a) Δt = 0 CPP
Rel. ionization eff.
4.0
2.0
0.0
200
150
100
50
0
Pulse width, FWHM (fs)
250
500
750
1000
State lifetime, τ (fs)
(b) Δt = 0 CAP
Rel. ionization eff.
1.5
1.0
0.5
200
150
100
50
0
Pulse width, FWHM (fs)
250
500
750
1000
State lifetime, τ (fs)

Fig 2

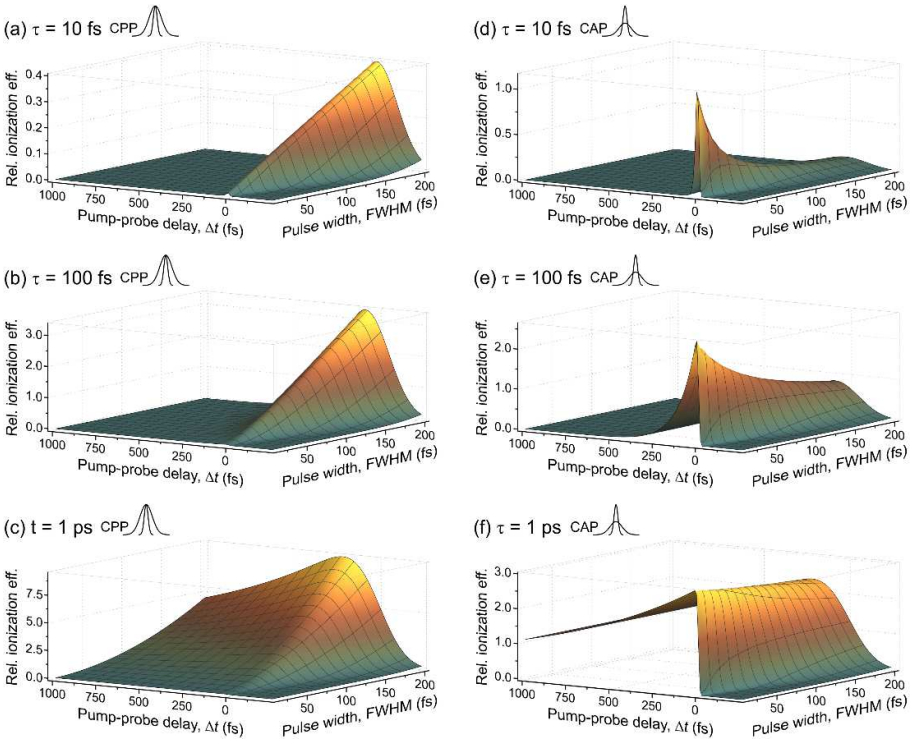
(a) τ = 10 fs CPP
(b) τ = 100 fs CPP
(c) t = 1 ps CPP
(d) τ = 10 fs CAP
(e) τ = 100 fs CAP
(f) τ = 1 ps CAP
Rel. ionization eff.
Pump-probe delay, Δt (fs)
Pulse width, FWHM (fs)

Fig 3

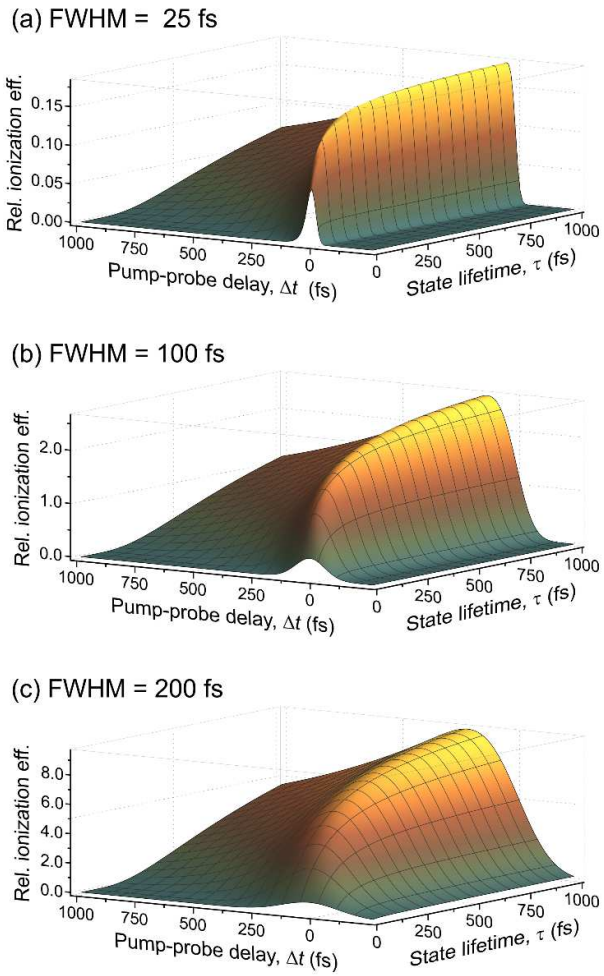
(a) FWHM = 25 fs
Rel. ionization eff.
0.15
0.10
0.05
0.00
1000
750
500
250
0
Pump-probe delay, Δt (fs)
0
250
500
750
1000
State lifetime, τ (fs)
(b) FWHM = 100 fs
Rel. ionization eff.
2.0
1.0
0.0
1000
750
500
250
0
Pump-probe delay, Δt (fs)
0
250
500
750
1000
State lifetime, τ (fs)
(c) FWHM = 200 fs
Rel. ionization eff.
8.0
6.0
4.0
2.0
0.0
1000
750
500
250
0
Pump-probe delay, Δt (fs)
0
250
500
750
1000
State lifetime, τ (fs)

Fig 4

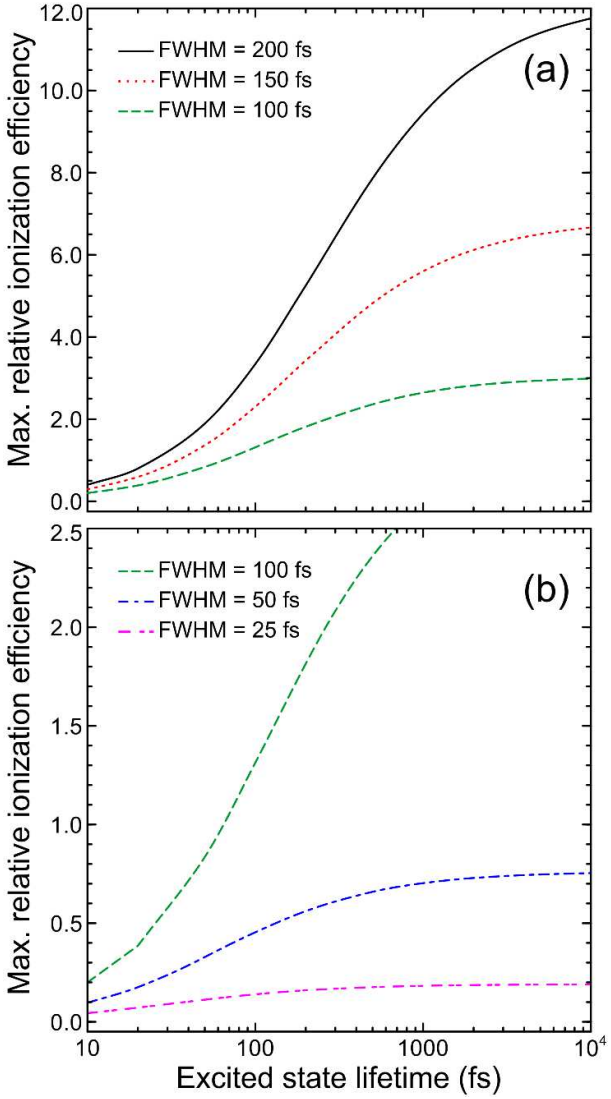
FWHM = 200 fs
FWHM = 150 fs
FWHM = 100 fs
(a)
Max. relative ionization efficiency
12.0
10.0
8.0
6.0
4.0
2.0
0.0
FWHM = 100 fs
FWHM = 50 fs
FWHM = 25 fs
(b)
Max. relative ionization efficiency
2.5
2.0
1.5
1.0
0.5
0.0
10
100
1000
10^4
Excited state lifetime (fs)

Fig 5

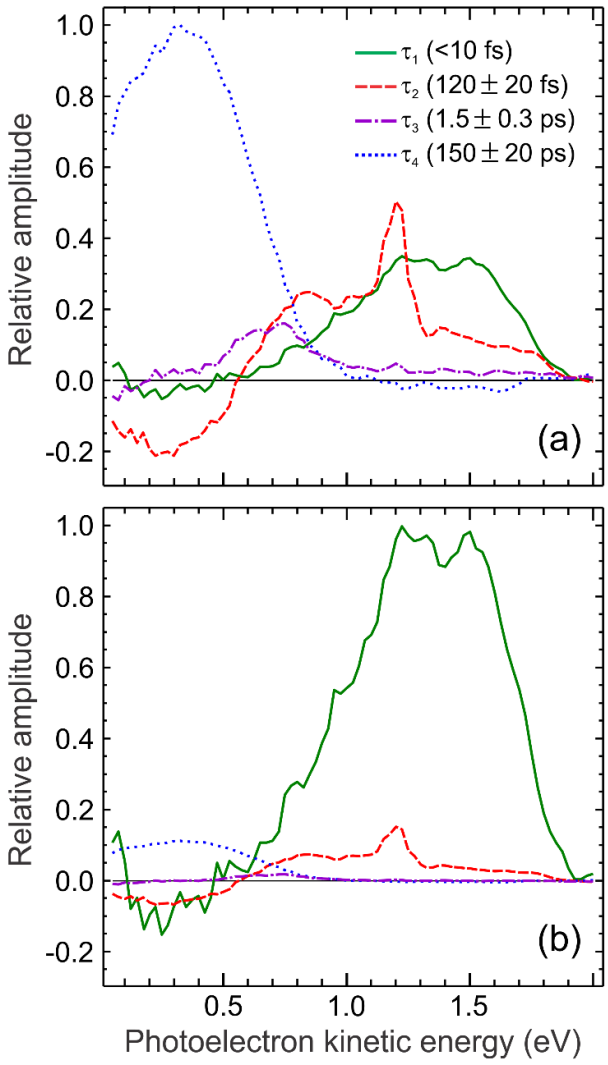
τ1 (<10 fs)
τ2 (120 ± 20 fs)
τ3 (1.5 ± 0.3 ps)
τ4 (150 ± 20 ps)
Relative amplitude
(a)
(b)
Photoelectron kinetic energy (eV)

Fig 6

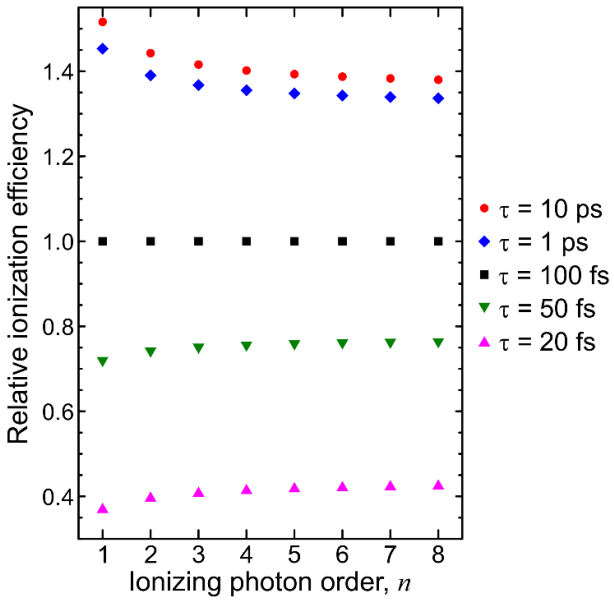
Relative ionization efficiency
1.4
1.2
1.0
0.8
0.6
0.4
1
2
3
4
5
6
7
8
Ionizing photon order, n
τ = 10 ps
τ = 1 ps
τ = 100 fs
τ = 50 fs
τ = 20 fs

Fig 7

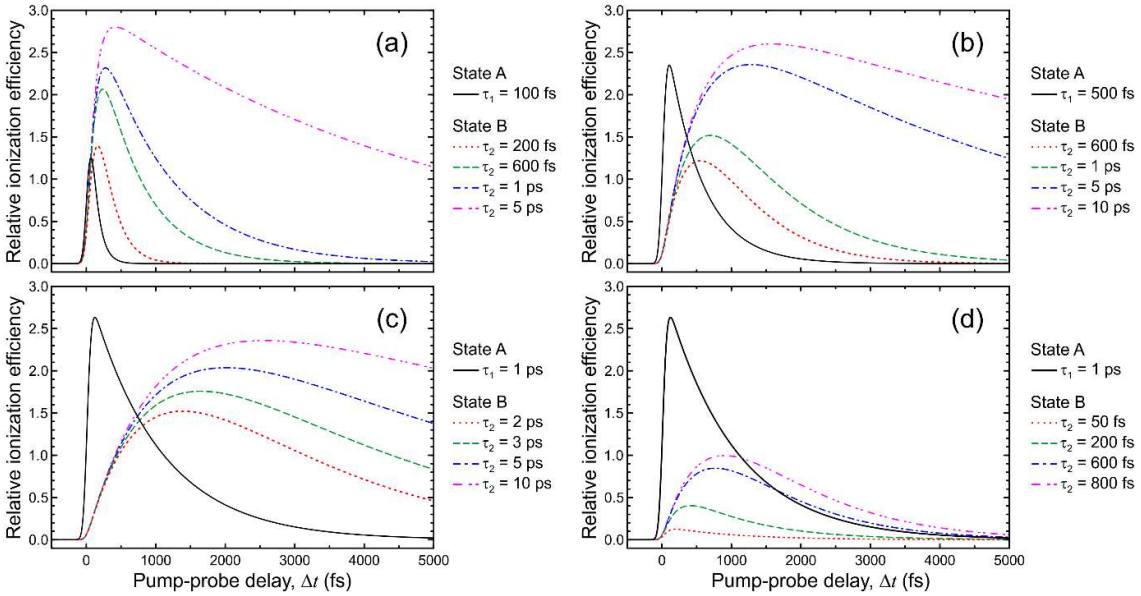
(a)
(b)
(c)
(d)
Relative ionization efficiency
Pump-probe delay, Δt (fs)
State A
τ1 = 100 fs
State B
τ2 = 200 fs
τ2 = 600 fs
τ2 = 1 ps
τ2 = 5 ps
State A
τ1 = 500 fs
State B
τ2 = 600 fs
τ2 = 1 ps
τ2 = 5 ps
τ2 = 10 ps
State A
τ1 = 1 ps
State B
τ2 = 2 ps
τ2 = 3 ps
τ2 = 5 ps
τ2 = 10 ps
State A
τ1 = 1 ps
State B
τ2 = 50 fs
τ2 = 200 fs
τ2 = 600 fs
τ2 = 800 fs